Chinese Journal of Natural Medicines

R–type ginsenoside Rg3 attenuates cisplatin–induce intestinal injury via restoring autophagy flux blockade

Xufei Gao, Junjie Zhang, Junnan Hu, Ming Zhang, Zi Wang, Shuang Jiang, Wei Li

Citation: Xufei Gao, Junjie Zhang, Junnan Hu, Ming Zhang, Zi Wang, Shuang Jiang, Wei Li, *R*–type ginsenoside Rg3 attenuates cisplatin–induce intestinal injury *via* restoring autophagy flux blockade, Chinese Journal of Natural Medicines, 2026, 24(4), 485–498. doi: 10.1016/S1875–5364(26)61100–4.

View online: https://doi.org/10.1016/S1875–5364(26)61100–4

Chinese Journal of Natural Medicines 24 (2026) 485-498

Contents lists available at ScienceDirect

Chinese Journal of Natural Medicines

journal homepage: www.cjnmcpu.com/

Original article

R-type ginsenoside Rg3 attenuates cisplatin-induce intestinal injury *via* restoring autophagy flux blockade

Xufei Gao[a], Junjie Zhang[a], Junnan Hu[a], Ming Zhang[b], Zi Wang[a,*], Shuang Jiang[a,*], Wei Li[a,c,*]

[a] *College of Chinese Medicinal Materials, Jilin Provincial International Joint Research Center for the Development and Utilization of Authentic Medicinal Materials, Jilin Agricultural University, Changchun 130118, China*

[b] *College of Medicine, Jilin University, Changchun 130021, China*

[c] *Engineering Research Center of the Chinese Ministry of Education for Bioreactor and Pharmaceutical Development, Jilin Agricultural University, Changchun 130118, China*

ARTICLE INFO

Article history:
Received 27 May 2025
Revised 28 July 2025
Accepted 4 August 2025
Available online 20 April 2026

Keywords:
R-Ginsenoside Rg3
Cisplatin
Lysosomal dysfunction
Autophagic flux blockade.

ABSTRACT

Cisplatin and its metabolites can cause severe gastrointestinal mucosal damage, leading to varying degrees of intestinal injury in nearly all patients following administration. Although the anti-tumor effectiveness of *R*-ginsenoside Rg3 (*R*-Rg3, a key chemical component of Shen Yi Capsule) as the first-line drug is widely recognized in the clinic, there is less concern about the improved effects of *R*-Rg3 against intestinal toxicity caused by concurrent cisplatin chemotherapy. This study aimed to investigate the protective effects of *R*-Rg3 against cisplatin-induced intestinal toxicity and to explore its potential molecular targets and mechanisms. Rats in the *R*-Rg3 treatment group were treated with *R*-Rg3 (7, 14 mg·kg^{-1}, p.o.) for 7 days, and a single dose of cisplatin (14 mg·kg^{-1}, i.p.) was administered *via* intraperitoneal injection to rats in the cisplatin group and *R*-Rg3 treatment group on the 7th day. Intestinal epithelial cell line 6 (IEC-6) were pretreated with *R*-Rg3 (1.25, 2.5, 5 μmol·L^{-1}) for 24 h followed by cisplatin treatment (3 μmol·L^{-1}, 24 h). The *in vivo* results showed that, *R*-Rg3 treatment for 7 days markedly alleviated cisplatin-induced oxidative stress and mitochondrial dysfunction in vivo, while suppressing excessive autophagy and reducing intestinal damage. In IEC-6 cells, R-Rg3 pretreatment inhibited mitophagy and promoted the restoration of lysosomal function. Autophagy inhibitors 3-methyladenine (autophagosome formation inhibitor, 1 μmol·L^{-1}) and Bafilomycin A1 (proton pump inhibitor, 8 μmol·L^{-1}) were used to verify the mechanism of *R*-Rg3 action. Importantly, application of 3-methyladenine and Bafilomycin A1 verified that *R*-Rg3 could alleviate gastrointestinal dysfunction by restoring the cisplatin-induced autophagic flux blockade. In conclusion, this study identifies a previously underappreciated protective role of *R*-Rg3 against cisplatin-induced intestinal injury. Furthermore, it suggests that pharmacological modulation of the mitochondria–lysosome axis by *R*-Rg3 may effectively mitigate oxidative stress–mediated autophagic flux impairment caused by cisplatin.

1. Introduction

As a highly potent chemotherapeutic agent that damages DNA, cisplatin is extensively used in the treatment of various solid tumors [1–2]. Despite its remarkable efficacy, its associated toxicities and side effects substantially limit its therapeutic application [3]. Among these, gastrointestinal toxicity is particularly prevalent, with nearly all patients experiencing varying degrees of intestinal injury following cisplatin administration. This toxicity arises primarily from damage to the gastrointestinal mucosa caused by cisplatin and its metabolites, which not only compromises patient quality of life but may also necessitate dose reduction or discontinuation of chemotherapy [4]. The intestinal epithelium is especially susceptible to cisplatin-induced damage due to its rapid turnover and high metabolic activity. Clinically, this toxicity manifests as mucosal injury, gastrointestinal dysmotility, and vomiting, all of which negatively affect treatment adherence [5]. Furthermore, cisplatin demonstrates antimicrobial activity against both Gram-positive and Gram-negative bacteria. This effect disrupts the distribution and function of the intestinal microbiota (dysbiosis), ultimately leading to severe damage to the intestinal mucosa [6]. Therefore, in addition to nephrotoxicity and ototoxicity, the severe gastrointestinal toxicity should be given more attention as the primary prognostic reaction.

Accumulating evidence indicates that cisplatin induces excessive production of reactive oxygen species (ROS) after entering the body. This leads to lipid peroxidation, disruption of the antioxidant defense system, metabolic imbalance, and oxidative damage [7–8]. Consequently, excessive accumulation of lipid peroxides activates cellular stress responses, ultimately triggering cell death pathways, including apoptosis, necrosis, and autophagy [9–10]. Mitochondria, as the primary sites of cellular energy production, are particularly vulnerable to ROS accumulation. Oxidative damage to mitochondria not only impairs their structure and function but also promotes the formation of autophagosomes and disrupts autophagic flux [11]. When the autophagy process in-

* Corresponding author.
E-mail addresses: wangzi8020@126.com (Z. Wang); 124092069@qq.com (S. Jiang); liwei7727@126.com (W. Li)

https://doi.org/10.1016/S1875-5364(26)61100-4

creases, it causes damage to Caco-2 cells, which is mediated by the continuous activation of ROS-dependent ERK1/2 [12]. The main function of lysosomes is to help cells metabolize by taking in and dissolving unwanted cell parts, cell debris, or foreign bodies that enter the cell. Elevated ROS levels also can compromise lysosomal function, prompting cells to respond to oxidative stress by triggering autophagy [13] . It's worth noting that there is a strong association between the excessive occurrence of autophagy and lysosomal damage or dysfunction [14]. Consequently, blockade of autophagic flux due to impaired lysosomal function or excessive autophagy was found to be a target to address cisplatin-induced intestinal injury.

Natural products and their bioactive constituents have shown considerable potential in mitigating cisplatin-induced intestinal toxicity [15]. Ginsenosides, the primary active compounds in the roots of *Panax ginseng* C. A. Meyer, exhibit diverse pharmacological activities, including anti-diabetic, anti-cancer, and anti-inflammatory effects [16-17]. The steaming process may result in the conversion of considerable molecular weight and high polar saponin into small molecular weight and low polar saponin (Rg3, Rg5, Rk1, Rz1, F4, Rg6, etc.) [18]. Ginsenoside Rg3 (Rg3), a secondary ginsenoside derived from red ginseng (RG), exists in two epimeric forms: *S*-type ginsenoside Rg3 (*S*-Rg3) and *R*-type ginsenoside Rg3 (*R*-Rg3). Compared to *S*-Rg3, *R*-Rg3 exhibits lower polarity. This property makes *R*-Rg3 more conducive to intestinal absorption in humans [19]. Notably, *R*-Rg3 is a key chemical component of "Shen Yi Capsule", a novel anti-cancer drug in China. Building upon our prior studies [10] affirming the protective effect of RG against cisplatin-induced intestinal injury, we further investigated the molecular mechanisms by which *R*-Rg3 protects against cisplatin-induced intestinal toxicity. Given the clinical importance of reducing chemotherapy-associated toxicity, understanding the mechanisms of cisplatin-induced intestinal injury and identifying effective protective agents are of considerable significance. In this study, we established *in vivo* and *in vitro* models to explore the potential ameliorative effect of *R*-Rg3 on cisplatin-induced intestinal injury. Our aim was to clarify the role of *R*-Rg3 in preventing cisplatin-induced intestinal mucosal damage and to explore its underlying mechanisms, thereby providing a theoretical basis for improving chemotherapy safety and patient outcomes.

2. Materials and methods

2.1. Chemicals and reagents

R-Rg3 (purity ≥ 97.5%, HPLC-UV verified) was isolated from ginseng as previously described [20]. Cisplatin (purity ≥99%) came from Sigma-Aldrich (St. Louis, MO, USA). MedChemExpress Biotech provided 3-methyladenine (3-MA), Bafilomycin A1, and N-acetylcysteine (NAC), which we stored at −80 °C in the dark. Nanjing Jiancheng Bioengineering Research Institute (Nanjing, China) supplied kits for measuring oxidative stress markers (MDA, LDH, CAT, SOD) and H&E staining. Beyotime Biotechnology (Shanghai, China) was the source for BCA protein assay kits, Hoechst 33258, mitochondrial membrane potential and MPTP assay kits, and Lyso-Tracker Green. R&D Systems (Minneapolis, MN, USA) provided DAO ELISA kits. Roche Applied Science (Germany) supplied the TUNEL apoptosis detection kit. BOSTER Biological Technology (Wuhan, China) offered SABC-DyLight488/Cy3 immunofluorescence staining kits. Cell Signaling Technology (Danvers, MA, USA) supplied primary rabbit monoclonal antibodies against Occludin, ZO-1, Bax, Bcl-2, cytochrome C, caspases 3/9 (cleaved and total), GAPDH, Nrf2, HO-1, PINK1, ATG3/5/7, Cathepsin B, and p62. Abclonal Technology (Wuhan, China) provided LC3 and LAMP2 antibodies. DQ™ Red BSA was from Thermo Fisher (Sasse, USA).

2.2. Animal experiments

Male SPF Wistar rats (8 weeks old, weighing 250–260 g) were procured from YISI Experimental Animal Co., Ltd. (Changchun, China; Quality Certificate No. SCXK(JI)-2023-0002). The rats were acclimatized for one week under controlled conditions (temperature: 23.0 ± 2.0 °C, humidity: 60.0% ± 10.0%, 12-h light/dark cycle) [21]. All animal experiments were strictly conducted in accordance with Chinese legislation and the Guide for the Care and Use of Laboratory Animals (Approval number: 20230619003).

Rats (n = 10 per group) were randomly divided into four groups: Normal (0.05% CMC-Na vehicle), cisplatin (14 mg·kg^{-1}), Low-dose *R*-Rg3 (*R*-Rg3-L, 7 mg·kg^{-1}), and High-dose *R*-Rg3 (*R*-Rg3-H, 14 mg·kg^{-1}). The *R*-Rg3 dose was derived from preliminary studies [22], using the rat equivalent dose. *R*-Rg3 powder was dissolved in 0.05% CMC-Na. Both *R*-Rg3 groups received daily oral *R*-Rg3 for 10 d, while the Normal and cisplatin groups received the vehicle daily. On day 7, one hour after dosing, rats in the cisplatin and *R*-Rg3 groups received a single intraperitoneal cisplatin injection (14 mg·kg^{-1} in saline) to induce intestinal injury. Seventy-two hours post-cisplatin injection, rats were euthanized *via* abdominal aortic blood collection. Serum was obtained by centrifugation (3000 × g, 10 min, twice) and stored at −80 °C. Duodenal tissues (a representative site for injury) were immediately collected. Tissues were rinsed in cold saline, blotted dry, and a segment (about 2–3 cm) was fixed in 10% formalin. The remaining tissue was flash-frozen in foil and stored at −80 °C.

2.3. Cell culture and treatment

IEC-6 cells were cultured in Dulbecco's modified Eagle's medium (DMEM) supplemented with 10% fetal bovine serum (FBS) at 37 °C and 5% CO_2. Cells in the logarithmic growth phase were used for all experiments. Cells were seeded into two 6-well plates using complete medium (containing 10% FBS) and assigned to either 7 or 5 treatment groups as follows: Group 1 (Normal), Group 2 (*R*-Rg3 single treatment), Group 3 (NAC single treatment), Group 4 (cisplatin single treatment), Group 5 (cisplatin + *R*-Rg3), Group 6 (cisplatin + NAC/3-MA/Bafilomycin A1), and Group 7 (cisplatin + *R*-Rg3 + NAC/3-MA/Bafilomycin A1). Cells were pretreated with inhibitors for 30 min, and then *R*-Rg3 powder was dissolved in DMEM. After that, cells in groups 2, 5, and 7 were administered with *R*-Rg3 for 24 h. Subsequently, cells in groups 4, 5, 6, and 7 were treated with 3 μmol·L^{-1} cisplatin (dissolved in serum-free medium) and placed in an incubator (Thermo, Waltham, USA) at 37 °C with 5% CO_2 for 24 h to extract cell proteins for subsequent analysis.

2.4. Analysis of DAO and oxidative stress indicators

Serum diamine oxidase (DAO) activity serves as an indicator of intestinal epithelial cell maturity and integrity, indirectly reflecting the extent of intestinal mucosal damage [23]. Following the manufacturer's protocol (R&D Systems DAO ELISA kits), we sequentially added test samples, standards, and substrate solution to the ELISA plate. The reaction was stopped, and within 15 min, the optical density (OD) at 450 nm for each well was measured using a microplate reader (Bio-Tek Epoch2, CA, USA). Results were then calculated to determine serum DAO content.

Additionally, serum levels of superoxide dismutase (SOD), catalase (CAT), lactate dehydrogenase (LDH), and malondialdehyde (MDA) were quantified using commercial kits per the manufacturer's instructions to evaluate oxidative stress levels.

2.5. Histopathological examinations

Formalin-fixed intestinal tissues were dehydrated through

graded ethanol, cleared in xylene, and embedded in paraffin. Sections (5 μm) were prepared using a rotary microtome (Leica, RM2235, Solms, Germany) and stained with H&E. Histopathological changes were examined under a light microscope (Leica, DM750, Solms, Germany). Finally, intestinal villi injury and crypt loss were classified and scored based on their percentage using semi-quantitative methods.

2.6. Immunofluorescence staining

As described previously [24], 5-μm-thick intestinal tissue sections were deparaffinized and dehydrated. Sections underwent antigen retrieval in citrate buffer (0.01 mol·L^{-1}, pH 6.0) for 8 min, followed by three PBS washes. Non-specific staining was blocked by incubating sections with 1% bovine serum albumin (BSA) for 30 min. After removing excess liquid, primary antibodies against Bcl-2 and Bax (diluted 1∶200) were applied to sections and incubated overnight at 4 °C. The next day, sections were washed three times with PBS and then incubated with Dylight 488-labeled secondary antibody (1∶400) for 30 min in the dark. Subsequently, DAPI solution was added under identical conditions and incubated at room temperature for 20 min. Sections were then washed three times with PBS (10 min each). Finally, images were captured using a Leica TCS SP8 microscope (Germany) and analyzed using Image-Pro Plus 6.0 software (Media Cybernetics, USA).

2.7. Hoechst 33258 and TUNEL staining analysis

Apoptosis in intestinal tissues was evaluated using TUNEL staining and Hoechst 33258 analysis. Sections (5 μm thick) were treated with 10 μg·mL^{-1} Hoechst 33258 solution and subsequently washed three times with PBS (10 min per wash). Cell nuclear morphology and apoptotic status were then observed under dark conditions using a Leica microscope (Leica TCS SP8, Solms, Germany). Increased nuclear brightness indicated positive staining, and the ratio of positively stained cells to normal cells was calculated. For TUNEL staining, tissue sections underwent deparaffinization with xylene and rehydration through graded ethanol solutions prior to staining according to the manufacturer's protocol (TUNEL Apoptosis Detection Kit, Roche Applied Science, Shanghai, China).

2.8. Eukaryotic reference transcriptome

Total RNA was isolated from duodenum using TRIzol® Reagent (Magen) following the manufacturer's protocol. RNA quality was assessed using a Nanodrop ND-2000 (A260/A280 ratio) and an Agilent Bioanalyzer 4150 (RIN values). Only high-quality RNA was used for library construction. Differentially expressed genes (DEGs) were identified using DESeq2 ($|\log_2 FC| > 1$ and $P_{adj} < 0.05$). KEGG pathway enrichment analysis of DEGs was conducted using clusterProfiler to identify functionally enriched pathways (significance threshold: $P < 0.05$).

2.9. ROS staining

The relative intracellular ROS levels can be determined by fluorescence assays (DCFH -DA assays, Wanlei Biotechnology, China). IEC-6 cells were inoculated in a 6-well plate containing 10% FBS complete medium and grew in an incubator until the logarithmic growth phase. After successive treatments with *R*-Rg3 and cisplatin, the IEC-6 cells were incubated with 1.0 μmol·L^{-1} DCFH-DA for 30 min at 37 °C in the dark. After 30 min, we removed the medium and washed the cells with PBS 3 times to sufficiently remove DCFH-DA that did not enter the cells. After that, the 6-well plate was placed on the Leica microscope (Leica, DMIL LED, Germany) for imaging.

2.10. Mitochondrial membrane potential detection (JC-1)

Cells were plated in a 6-well plate and treated sequentially with *R*-Rg3 and cisplatin. The culture medium was discarded, and cells were washed once with 1 mL PBS. Subsequently, 1 mL of cell culture medium and 1 mL of JC-1 working solution were added to each well. After gentle mixing, the plate was incubated at 37 °C for 20 min. Following incubation, the supernatant was aspirated, and cells were washed twice with JC-1 staining buffer (10 min per wash). Mitochondrial membrane potential changes were analyzed using a fluorescence microscope (Leica DMIL LED, Germany).

2.11. Detection of cell apoptosis and MPTP

Cells were seeded in 6-well plates and treated with *R*-Rg3 and cisplatin. After treatment, cells were trypsinized and transferred to 2 mL centrifuge tubes. The cells were washed with 1–2 mL PBS and centrifuged at 300 × g for 10 min (15 mL tube), after which the supernatant was discarded. The cell pellet was resuspended in 100 μL of 1× binding buffer. Subsequently, 5 μL of FITC was added, gently mixed, and incubated in the dark for 10 min. Then, 5 μL of propidium iodide (PI) was added, mixed, and incubated in the dark for an additional 5 min. Finally, 300–500 μL PBS was added, and the samples were gently mixed prior to flow cytometry analysis.

For mitochondrial permeability transition pore (MPTP) analysis, samples underwent the same initial processing as described for apoptosis detection. After trypsinization and centrifugation (1000 × g, 5 min), the supernatant was discarded. Cells were resuspended in detection buffer containing Calcein AM staining solution, fluorescence quenching working solution, or Ionomycin control (for single-cell suspensions at 1 × 10^6 cells/mL; 1 mL per sample). A negative control group (detection buffer only) was included. Samples were incubated at 37 °C for 30 min in the dark. After incubation, cells were centrifuged (1000 × g, 5 min), washed with 1 mL detection buffer, and centrifuged again. The final cell pellet was resuspended in 400 μL detection buffer. Samples were kept on ice and analyzed by flow cytometry within 1 h.

2.12. Western blotting analysis

To investigate *R*-Rg3's protective mechanism against cisplatin-induced intestinal injury, we analyzed pathway proteins by western blotting [25]. We homogenized intestinal tissues or IEC-6 cells in RIPA buffer containing protease to extract proteins. Equal protein amounts underwent separation *via* 6%–15% SDS-PAGE and were electrophoretically transferred to PVDF membranes. Membranes were blocked with 5% BSA for 2 h at room temperature and then washed three times with TBST (5 min each). The membranes were incubated overnight at 4 °C with primary antibodies against Occludin Occludin (1∶1000), ZO-1 (1∶1000), Bax (1∶2000), Bcl-2 (1∶2000), cyt-C (1∶1000), caspase 9 (1∶1000), cleaved-caspase 9 (1∶1000), caspase 3 (1∶1000), cleaved-caspase 3 (1∶1000), GAPDH (1∶2000), Nrf2 (1∶1000), HO-1 (1∶1000), PINK1 (1∶2000), Parkin (1∶1000), LC3 (1∶1000), ATG3 (1∶1000), ATG5 (1∶1000), ATG7 (1∶1000), LAMP2 (1∶2000), Cathepsin B (1∶1000), and p62 (1∶1000). After washing with TBST, membranes were incubated with HRP-conjugated secondary antibodies for 1 h at room temperature. Protein bands were visualized using an enhanced chemiluminescence (ECL) substrate and quantified using Image-Pro Plus 6.0 software.

2.13. Lysosomal function assessment

(1) A 1 mg·mL^{-1} stock solution of DQ™ Red BSA was pre-

pared by dissolving the contents of the vial in 1 mL PBS buffer at an appropriate pH (pH 7.0–8.0). Cells were incubated with the staining solution for 2 h. After incubation, the medium was discarded, and cells were washed with prewarmed PBS buffer 1–2 times (5 min each wash).

(2) Lyso-Tracker Green working solution was prepared by adding 1 μL Lyso-Tracker Green to 13.33 mL of cell culture medium. After removal of the original culture medium, cells were incubated with the prewarmed Lyso-Tracker Green working solution at 37 °C for 30 min. The staining solution was then removed, and fresh culture medium was added.

Fluorescence images were subsequently captured using an inverted fluorescence microscope (Leica DMIL LED, Germany).

2.14. Statistical analysis

All data are presented as mean ± standard deviation (Mean ± SD) derived from independent experiments. Statistical analyses were performed using one-way analysis of variance (ANOVA) followed by Bonferroni post hoc test. Histopathological data were analyzed using a nonparametric test (Ridit analysis). Statistical graphs were generated using GraphPad Prism 8.0.2 software (GraphPad Software, Inc., San Diego, USA). A value of $P < 0.05$ was considered statistically significant.

3. Results

3.1. R-Rg3 ameliorated cisplatin-induced intestinal mucosal damage in rats

As depicted in Fig. 1A, rats in the cisplatin group (14 $mg \cdot kg^{-1}$) exhibited a progressive decline in body weight compared with the normal group. This weight loss was significantly alleviated by R-Rg3 treatment, particularly at the high dose ($P < 0.05$ or $P < 0.01$). Serum DAO level is an important indicator reflecting the integrity of the intestinal wall structure (Fig. 1B). The results showed that DAO level was significantly elevated in the cisplatin group, indicating severe damage to the intestinal wall tissue structures ($P < 0.01$). In contrast, DAO level in the high-dose R-Rg3 group was significantly reduced compared with that in the cisplatin group ($P < 0.01$). In addition, the expression levels of Occludin and ZO-1, which reflect intestinal tight junction integrity and barrier damage, were significantly upregulated by R-Rg3 treatment in rats with cisplatin-induced intestinal injury ($P < 0.05$ or $P < 0.01$; Figs. 1C–1D).

H&E staining was subsequently used to further evaluate the protective effect of *R*-Rg3 on cisplatin-induced mechanical barrier damage. As shown in Fig. 1E, intestinal absorptive cells in the normal group were neatly arranged, with the brush border appearing as obvious thin strips. Intestinal crypt cells remained intact, and vacuolated goblet cells were evenly distributed on the surfaces of both crypts and villi. After cisplatin exposure, intestinal epithelial cells became irregularly arranged and showed evident mucosal injury. The intestinal glands were markedly distorted, villus length was reduced, and crypt cells were notably ablated, indicating severe intestinal injury ($P < 0.01$). In contrast, the small intestinal absorption cells in the *R*-Rg3-H group exhibited a neatly arrangement. The damage of crypt cells and goblet cells were reduced, and the extent of distortion in intestinal glands was notably less than that observed in the cisplatin group ($P < 0.01$). These results indicated that supplementation of *R*-Rg3 could protect the intestine from cisplatin-induced intestinal mechanical barrier breakage.

Apoptosis, a highly regulated process of cell loss, holds a pivotal role in maintaining the homeostasis of body tissues. As depicted in Figs. 2A–2B, cisplatin substantially elevated the expression of key apoptosis executors (cyt-C), apoptotic proteases (caspase 3, and Bax). Following 10 days of oral administration of *R*-Rg3, the overexpression of these pro-apoptotic proteins was significantly reversed, accompanied by upregulation of the anti-apoptotic protein Bcl-2. Analysis of Hoechst 33258 and TUNEL results (Figs. 2A–2B) revealed a significantly higher apoptotic rate of intestinal epithelial cell nuclei in the cisplatin group than in the normal group ($P < 0.01$). Notably, *R*-Rg3 treatment markedly alleviated the cisplatin-induced positivity of Hoechst 33258 and TUNEL cell expression levels ($P < 0.01$). Immunofluorescence also revealed similar results (Figs. 2C–2D). Consistently, similar changes in apoptosis-related protein expression were observed at the cellular level (Figs. 2E–2F). Flow cytometry further demonstrated that the apoptosis rate induced by cisplatin was significantly attenuated after treatment with *R*-Rg3 (Figs. 2G–2H) ($P < 0.01$ or $P < 0.001$).

3.2. R-Rg3 alleviated ROS-mediated mitochondrial dysfunction and inhibited autophagy

Transcriptome analysis was performed comparing the cisplatin group with the normal group (Figs. 3A–3B). Enrichment analysis of differentially expressed genes showed significant association with oxidative stress-related pathways, suggesting that alleviation of oxidative stress and mitochondrial dysfunction may underlie the therapeutic effect of *R*-Rg3 against cisplatin-induced intestinal toxicity. As shown in Figs. 3C–3E, the cisplatin group exhibited significantly reduced antioxidant enzyme activities, including SOD and CAT, together with a marked increase in MDA content ($P < 0.01$ or $P < 0.001$), which showed severe oxidative damage. In contrast, the *R*-Rg3 group reversed this phenomenon ($P < 0.05$ or $P < 0.01$). At the same time, the *in vitro* results showed that *R*-Rg3 dose-dependently reduced the increase in MDA content and LDH activity in IEC-6 cells induced by cisplatin while recovering SOD activity (Figs. 3F–3H) ($P < 0.05$ or $P < 0.01$). Similarly, in Figs. 3I–3J, *R*-Rg3 dose-dependently reduced intracellular ROS levels.

Oxidative stress readily induces mitochondrial damage and disrupts mitochondrial homeostasis, thereby affecting cellular processes. The PINK1/Parkin signaling pathway plays a critical role in mitochondrial dysfunction. When mitochondria are damaged, PINK1 activates Parkin to initiate autophagy. In addition, Parkin-mediated ubiquitination promotes targeted recruitment of LC3, thereby facilitating autophagy. As illustrated in Figs. 4A–4B, cisplatin significantly upregulated the expression of PINK1 and Parkin proteins in the duodenum ($P < 0.01$ or $P < 0.001$), and this response was effectively reversed by *R*-Rg3 treatment ($P < 0.001$). To investigate whether *R*-Rg3 can mitigate cisplatin-induced autophagy, we conducted immunofluorescence analysis for the autophagy marker (LC3). As depicted in Figs. 4C–4D, *R*-Rg3 significantly reduced the fluorescence intensity of the LC3 protein ($P < 0.01$), suggesting that *R*-Rg3 may intervene in the autophagy process. Consistent with the *in vivo* findings *R*-Rg3 also alleviated the cisplatin-induced overexpression of PINK1, Parkin, and LC3 *in vitro* (Figs. 4E–4F) ($P < 0.05$, $P < 0.01$, or $P < 0.001$). Assessment of mitochondrial permeability transition pore (MPTP) opening and JC-1 staining further showed that *R*-Rg3 effectively restored mitochondrial function and concomitantly reduced apoptosis (Figs. 4G–4H). The above results suggested that *R*-Rg3 ameliorates cisplatin-induced oxidative stress-mediated mitochondrial dysfunction and suppresses autophagy. Moreover, since autophagy can trigger programmed cell death and apoptosis is itself a programmed cell death process, these findings are consistent with the previous apoptosis results.

To examine the pivotal role of oxidative stress in cisplatin-induced injury, we introduced NAC, a ROS inhibitor, and assessed the protein expression related to oxidation, autophagy, and apop-

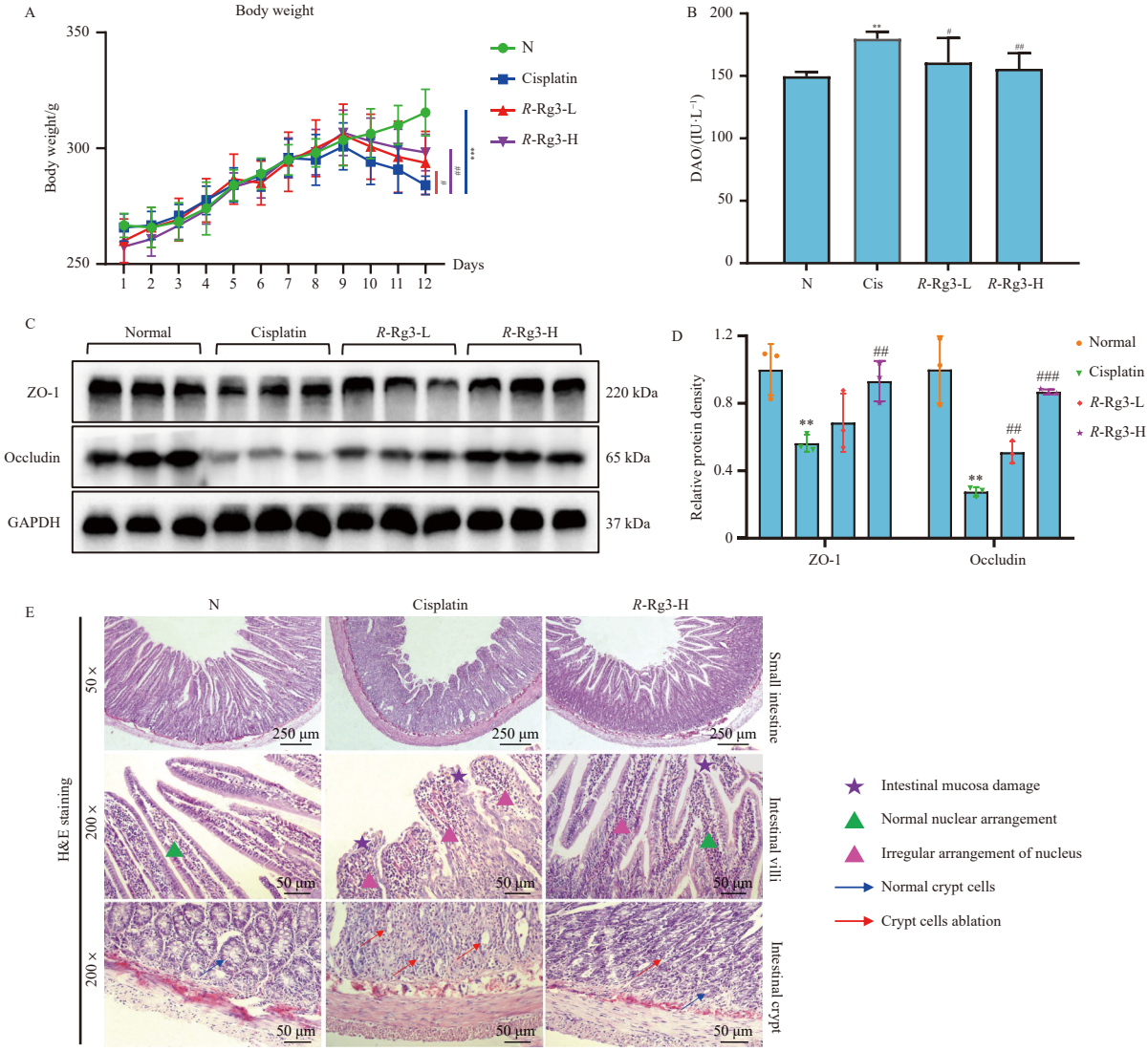

Fig. 1 *R*-Rg3 ameliorated cisplatin-induced intestinal barrier damage. (A) Changes in body weight. (B) DAO level. (C) Protein expression of Occludin and ZO-1. (D) Histogram analysis of Occludin and ZO-1 protein expression levels. (E) H&E staining of intestinal tissues (50×, 200×). Note: Intestinal mucosa damage (purple five-pointed star); normal nuclear arrangement (green triangle), irregular nuclear arrangement (pink triangle); normal crypt cell (blue arrow), crypt cell ablation (red arrow). All values are expressed as mean ± SD (n = 3 in each group). $^{**}P < 0.01$ *vs* normal (N) group; $^{\#}P < 0.05$, $^{\#\#}P < 0.01$ *vs* cisplatin (Cis) group.

tosis. As depicted in Fig. 5, NAC significantly reduced ROS production and concurrently increased the expression of Nrf2 and its cytoprotective downstream enzyme HO-1, both key regulators of oxidative stress response genes ($P < 0.05$ or $P < 0.01$). Simultaneously, NAC markedly restrained the protein expression levels of autophagy factors (ATG5, ATG7, LC3) and apoptotic factors (caspase 3 and Bax), while augmenting the expression levels of the anti-apoptotic factor Bcl-2 protein ($P < 0.05$, $P < 0.01$, or $P < 0.001$). These results demonstrated at the cellular level that oxidative stress is a pivotal target influencing autophagy and apoptosis. *R*-Rg3 and NAC collaboratively inhibited oxidative stress occurrence, thereby mitigating cisplatin-induced damage.

3.3. R-Rg3 promoted the restoration of lysosomal function and relieved autophagy flux blockade to ameliorate intestinal injury

The regulatory effect of *R*-Rg3 on autophagy in intestinal tissue was detected. The results showed that *R*-Rg3 treatment markedly suppressed the protein expression levels of ATG3, ATG5 and ATG7 (Figs. 6A–6B, $P < 0.01$, or $P < 0.001$). Furthermore, *R*-Rg3 exhibited a notable dose-dependent attenuation of cisplatin-induced overexpression of autophagic proteins in the *in vitro* model of cisplatin-induced injury (Figs. 6C–6D, $P < 0.05$, $P < 0.01$, or $P < 0.001$). The p62 protein plays a pivotal role in intracellular waste clearance and maintenance of cellular homeostasis. In the cisplatin-treated group, p62 protein expression was elevated, indicating accumulation of autophagosomes induced by cisplatin. Subsequent treatment with *R*-Rg3 resulted in a significant reduction in the expression of p62 protein (Figs. 6E–6F), suggesting that *R*-Rg3 effectively mitigates cisplatin-induced autophagosome accumulation in IEC-6 cells in a dose-dependent manner ($P < 0.05$, $P < 0.01$, or $P < 0.001$). The accumulation of autophagosomes in cells is often caused by impaired fusion with lysosomes [26]. We therefore speculated that lysosomal function was impaired in the cisplatin group, preventing effective fusion with accumulated autophagosomes and leading to autophagosome buildup. Analysis of lysosomal functional proteins, including LAMP2 and Cathepsin B, supported this hypothesis (Figs. 6E–6F), and *R*-Rg3 demonstrated a dose-dependent restoration of lysosomal function, aligning with our speculation ($P < 0.05$, $P < 0.01$, or $P < 0.001$). Moreover, we evaluated lysosomal function through DQ^{TM} Red BSA and Lyso-Tracker Green staining (Figs. 6G–6H). The groups treated with different doses of *R*-Rg3 exhibited stronger fluorescence of DQ^{TM} Red BSA/Lyso-Tracker Green compared to the cisplatin-treated group ($P < 0.01$, or $P < 0.001$). This fluorescence enhancement indicated that *R*-Rg3 effectively promotes lysosomal digestion function and enhances lysosomal acidity in IEC-6 cells in a dose-dependent manner.

3-MA inhibits the initiation of autophagy, while Bafilomycin acts downstream of autophagy by inhibiting acidification, protein degradation within cellular lysosomes, and blocking the binding of autophagosomes and lysosomes. The results revealed that in the cisplatin combined with 3-MA group, the levels of autophagy marker proteins (ATG3, ATG5, ATG7 and LC3) were markedly lower than those in the cisplatin alone group, providing evidence that 3-MA could effectively block the initiation of autophagy. In Figs. 7A–7B, following treatment with *R*-Rg3 or 3-MA, the autophagy marker protein exhibited a significant reduction, and in the *R*-Rg3 combined with 3-MA treatment group, the autophagy protein level was further diminished ($P < 0.05$, $P <$

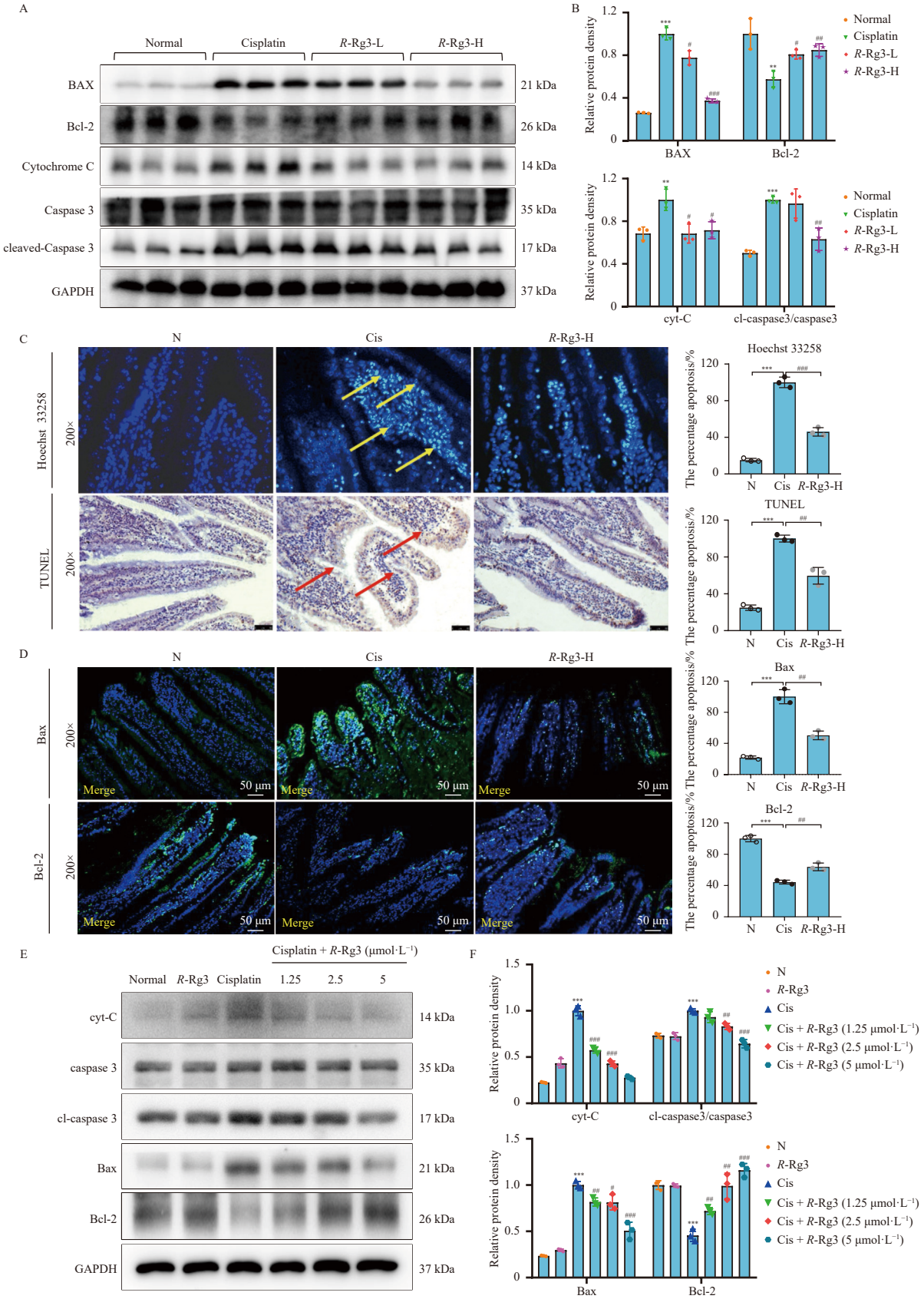

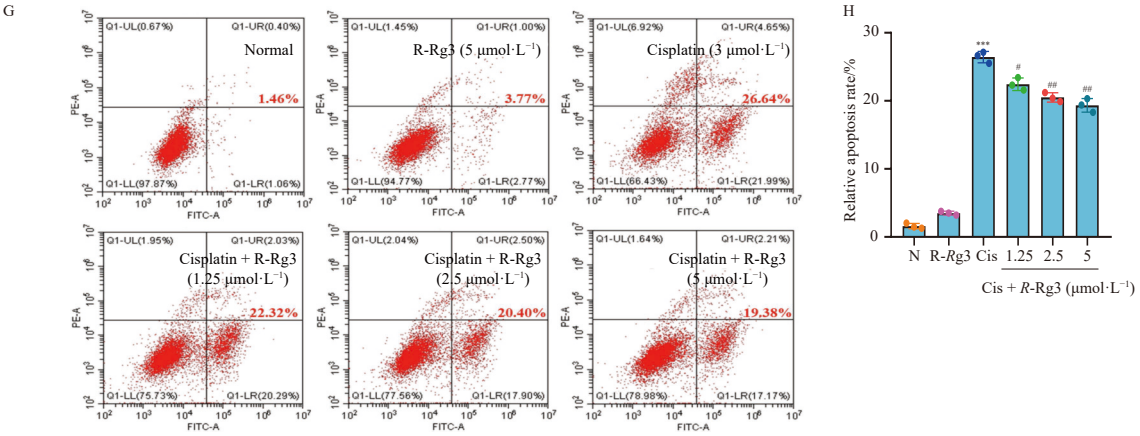

Fig. 2 *R*-Rg3 inhibited cisplatin-induced apoptosis *in vivo* and *in vitro*. (A) Effect of Rg3 on the expression levels of apoptosis-related proteins *in vivo*. (B) Histogram analysis of apoptosis-related proteins expression levels. (C) Hoechst 33258 and TUNEL staining of intestinal tissues (200×). Note: Apoptotic nuclei in the cisplatin group (yellow arrow) and TUNEL-positive cells (red arrow), with quantitative relative fluorescence intensity analysis of Hoechst 33258 and TUNEL staining. (D) Expression levels of Bax and Bcl-2 in tissue sections isolated from different groups, determined by immunofluorescence, with quantitative relative fluorescence intensity analysis of Bax and Bcl-2. (E) Effect of *R*-Rg3 on the expression levels of apoptosis-related proteins *in vitro*. (F) Histogram analysis of apoptosis-related protein expression levels. (G) Flow cytometric analysis of the effect of *R*-Rg3 on cisplatin-induced apoptosis. (H) Histogram analysis of the effect of *R*-Rg3 on cisplatin-induced apoptosis. All values are expressed as mean ± SD (n = 3 in each group). $^{**}P < 0.01$, $^{***}P < 0.001$ *vs* normal (N) group; $^{\#}P < 0.05$, $^{\#\#}P < 0.01$, $^{\#\#\#}P < 0.001$ *vs* cisplatin (Cis) group.

0.01, or $P < 0.001$). However, 3-MA treatment failed to increase the expression of lysosomal functional proteins LAMP2 and CTSB or decrease p62 expression, indicating that autophagic flux blockade still persisted (Figs. 7C–7D). This further confirmed that the cisplatin treatment disrupted the lysosomal function, while the *R*-Rg3 treatment reversed this phenomenon. To further support this conclusion, bafilomycin A1, a proton pump inhibitor, was also used. As shown in Figs. 7E–7F, in the presence of bafilomycin A1, the R-Rg3 + bafilomycin group showed significantly increased expression of lysosomal functional proteins compared with the cisplatin + bafilomycin group, accompanied by reduced p62 expression ($P < 0.01$, or $P < 0.001$). These findings suggest an antagonistic interaction between *R*-Rg3 and Bafilomycin. The results were further validated through DQ™ Red BSA and LysoTracker Green staining (Figs. 7G–7H, $P < 0.05$, $P < 0.01$, or $P < 0.001$). These results collectively confirm that *R*-Rg3 exerts intestinal protective function by upregulating lysosomal function and restoring the autophagy flux blockade induced by cisplatin.

4. Discussion

Cancer has become the number one killer that seriously threatens human health. In efforts to curb the rapid proliferation of tumor cells, a plethora of anti-cancer drugs has emerged. Among them, cisplatin, an inorganic platinum chemotherapeutic drug, stands out as a widely utilized treatment for various solid organ tumors [27-28]. However, as a cytotoxic drug, while effectively eliminating tumor cells, cisplatin also inflicts damage on normal human cells, particularly mucosal cells with a higher rate of proliferation, such as oral mucosa and gastrointestinal mucosa [29]. Mucosal damage triggers the generation of numerous ROS, disrupts the regular functioning of mitochondria, and sets off a cascade of molecular signaling pathways, including apoptosis and autophagy [30-32]. Our previous studies had substantiated that *R*-Rg3 possesses commendable antioxidant and anti-apoptotic activities [22], which provided an important entry point for us to study *R*-Rg3's antagonism of cisplatin intestinal toxicity. In this study, oxidative stress and its induced excessive autophagy play a key role in the intestinal toxic response induced by cisplatin. *R*-Rg3 can improve mitochondrial dysfunction, promote the recovery of lysosomal function by eliminating the high accumulation of oxygen free radicals, thus improving the intestinal injury caused by cisplatin.

To investigate the potential of *R*-Rg3 in modulating cisplatin-induced intestinal injury, our initial assessments involved monitoring the body weights and DAO levels of rats. Research has demonstrated that the elevated expression levels of serum DAO are indicative of damage and necrosis in intestinal mucosal cells [33]. Tight junction proteins, ZO-1 and Occludin, play a crucial role in sealing the gaps between adjacent epithelial cells, preventing the passage of bacteria and toxins produced in the intestinal lumen to reach the lamina propria [34-35]. Our results indicate that *R*-Rg3 treatment significantly increased the protein expression of ZO-1 and Occludin while reducing DAO levels. This suggests that *R*-Rg3 can decrease intestinal mucosal permeability and alleviate damage to the intestinal mucosal barrier. Combining these biochemical markers, it was not difficult to demonstrate that *R*-Rg3 treatment significantly reduced the mechanical barrier damage caused by cisplatin treatment. Moreover, we observed that *R*-Rg3 substantially attenuated cisplatin-induced alterations in the ultrastructure of intestinal villi and crypts.

Oxidative stress is a prevalent cytotoxic mechanism of cisplatin [36]. Cisplatin induces oxidative stress by generating ROS such as hydroxyl free radicals, superoxide, etc. Oxidative stress induces lipid peroxidation of polyunsaturated fatty acids (PUFA) in intestinal epithelial cells, thereby destroying the structural integrity of the biofilm and diminishing the physiological function of cells, or even causing their loss [37]. This experiment confirmed that *R*-Rg3 treatment inhibited the production of ROS and restored the activity of antioxidant enzymes (SOD and CAT), demonstrating its ability to counteract cisplatin-induced oxidative stress. The content of MDA reflects the body's lipid peroxidation and indirectly indicates the degree of cell damage [38]. LDH is a stable cytoplasmic enzyme that is rapidly released outside the cells when the cell membrane is damaged, making it a reliable indicator of cell damage. The reduction of MDA and LDH indicated that the treatment of *R*-Rg3 reduced the destruction of biological macromolecules (such as proteins and lipids), thus supporting the report that *R*-Rg3 has been shown to have an excellent antioxidant effect. Nrf2/HO-1, a vital endogenous anti-oxidative stress pathway, plays a crucial role in responding to oxidative stress [39]. Elevated levels of ROS inhibit the expression of Nrf2, and as a downstream protein regulated by Nrf2, HO-1 can assist Nrf2 in attenuating cisplatin-induced oxidative stress. *R*-Rg3 and NAC acted synergistically and jointly activated the Nrf2-mediated antioxidant mechanism. Simultaneously, antagonizing oxidative stress can alleviate mitochondrial dysfunction and eliminate the aggravation of apoptosis caused by excessive autophagy, which verifies the pivotal role of oxidative stress in cisplatin injury.

Elevated levels of ROS can disrupt mitochondrial homeostas-

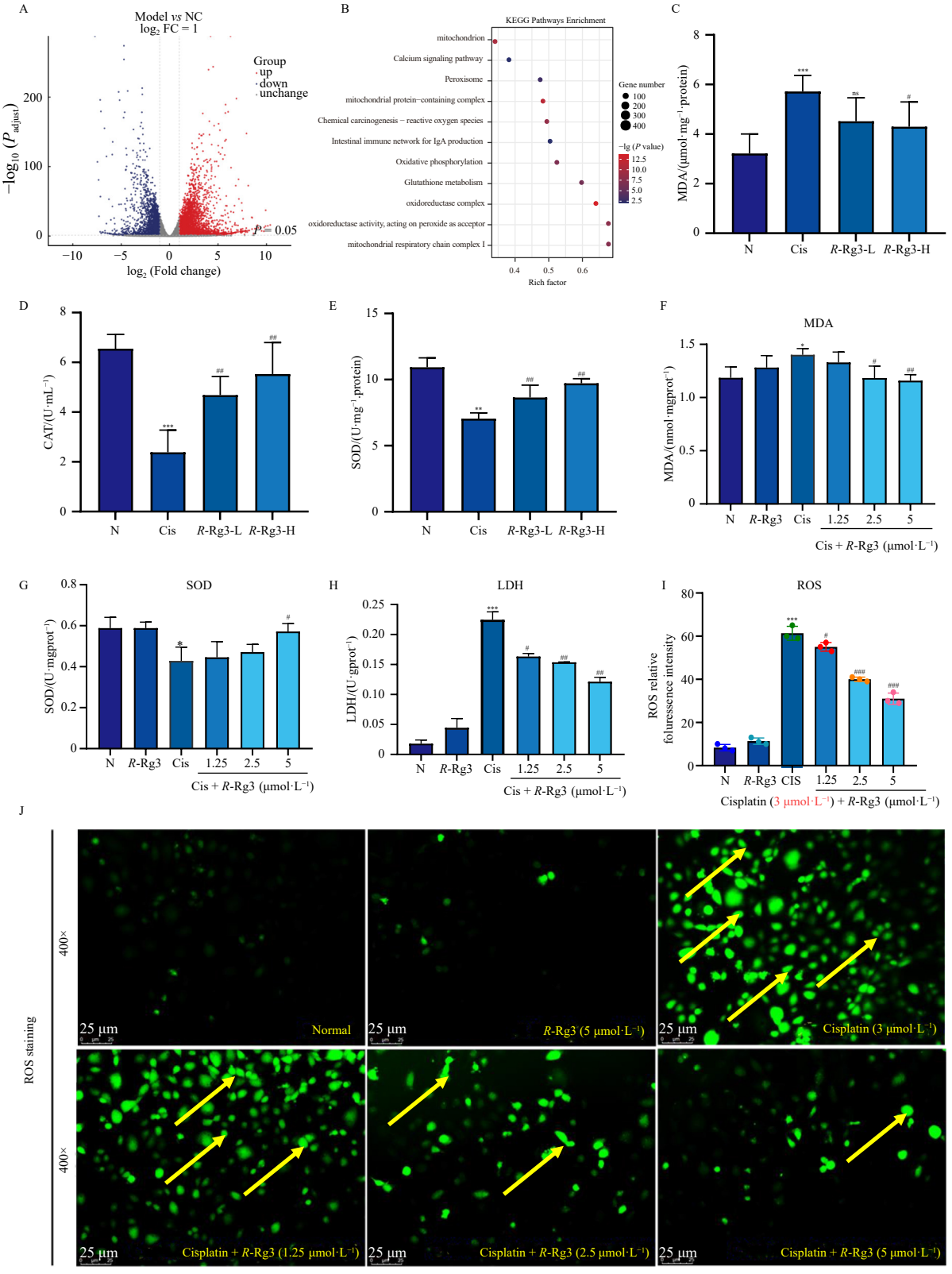

Fig. 3 *R*-Rg3 attenuated cisplatin-induced oxidative stress. (A) Differentially expressed genes. (B) KEGG analysis. (C) Intestinal MDA level. (D) Intestinal CAT level. (E) Intestinal SOD level. (F) Intracellular MDA level. (G) Intracellular SOD level. (H) Intracellular LDH level. (I) Effect of *R*-Rg3 on cisplatin-induced intracellular ROS generation (400 ×). Note: Yellow arrow indicates ROS fluorescence. (J) The histogram analysis of the relative fluorescence intensity of intracellular ROS in each group. All values are expressed as mean ± SD (n = 6 in each group). $^{*}P < 0.05$, $^{***}P < 0.001$ *vs* normal (N) group; $^{\#}P < 0.05$, $^{\#\#}P < 0.01$, $^{\#\#\#}P < 0.001$ *vs* cisplatin (Cis) group.

is, leading to cellular dysfunction [40–41]. Maintaining the balance of mitochondrial homeostasis requires processes such as mitochondrial fission (autophagy) [42], which plays a central role in mitochondrial quality control. PINK1, a protein kinase closely associated with mitochondrial function, plays a crucial role in regulating mitochondrial occurrence and functioning [43]. In this study, exposure to cisplatin made damaged mitochondria could not degrade PINK1, causing it to be abnormally activated. PINK1 was activated to promote the mitochondrial gene Parkin's recruitment and activation from the cytoplasm to the damaged mitochondrial outer membrane. Parkin ubiquitinates various proteins on the outer membrane of mitochondria, and selective auto-

phagy adaptor protein binds to ubiquitinated proteins and autophagy-related protein LC3-II, thus initiating autophagy degradation of damaged mitochondria. In the presence of *R*-Rg3, the change of the PINK1/Parkin signal was partially offset, indicating that *R*-Rg3 could improve mitochondrial dysfunction, thereby alleviating cisplatin damage and the results of JC-1 and MPTP also support this point.

Under normal circumstances, autophagy serves as a crucial mechanism for maintaining cellular homeostasis and adapting to environmental changes. Nevertheless, under certain circumstances, such as exposure to external stimuli, there can be aberrant activation of autophagy signaling pathways, leading to the

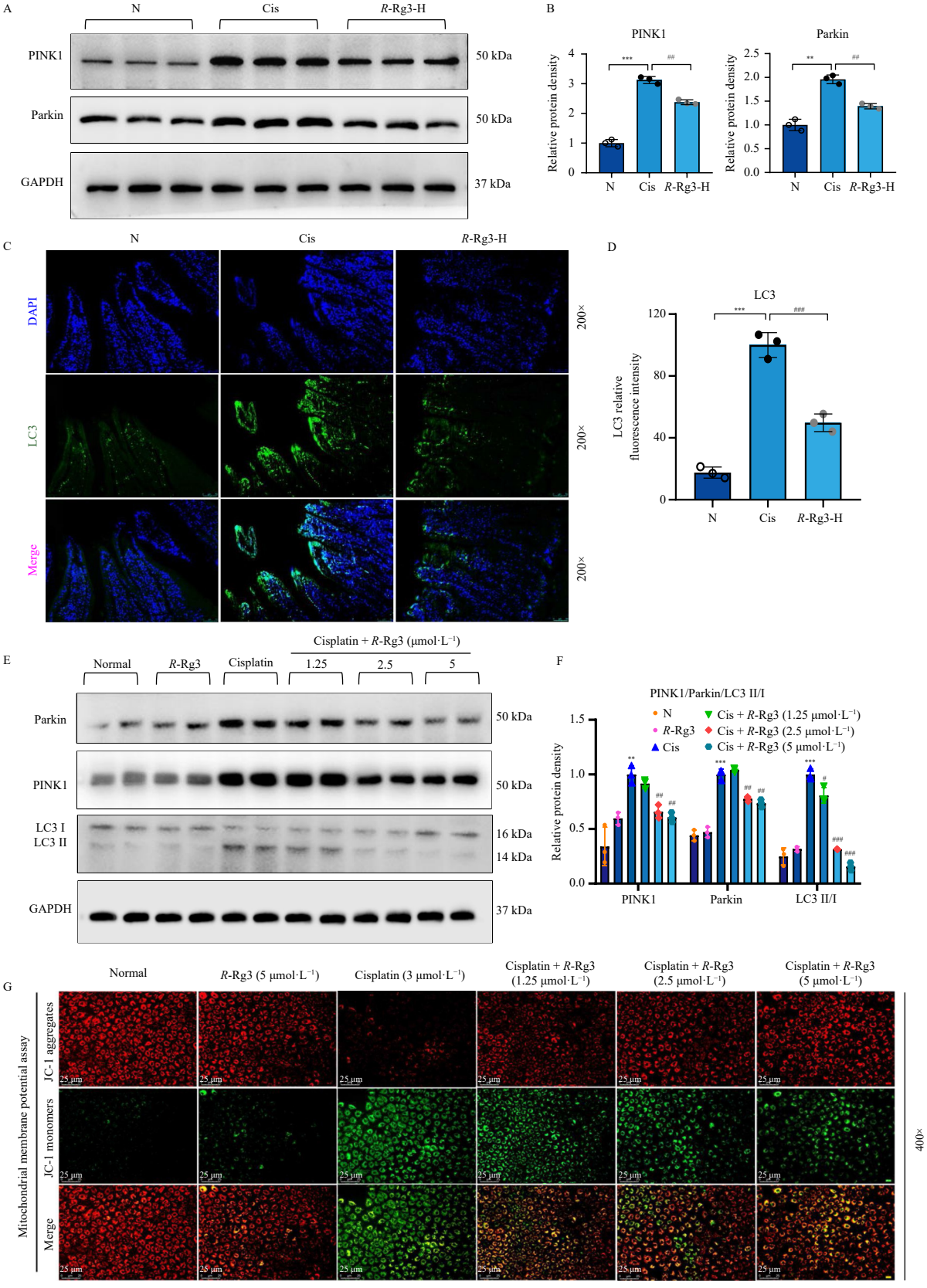

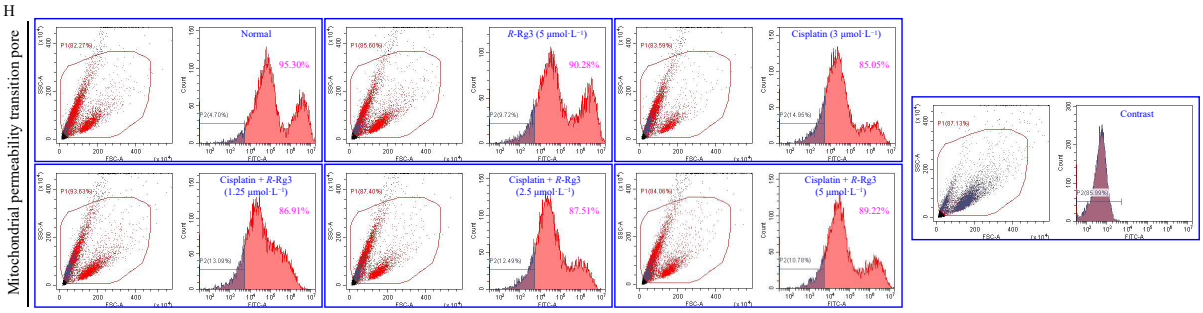

Fig. 4 *R*-Rg3 improved cisplatin-induced mitochondrial dysfunction. (A) Effect of *R*-Rg3 on protein expression levels of PINK1/Parkin signaling pathway *in vivo*. (B) Histogram analysis of Parkin/PINK1 protein expression levels. (C) Expression levels of LC3 in tissue sections isolated from different groups were determined by immunofluorescence (200×). (D) Histogram analysis of the relative fluorescence intensity of LC3 in each group. (E) Effect of *R*-Rg3 on protein expression levels of PINK1, Parkin, and LC3 *in vitro*. (F) Histogram analysis of PINK1, Parkin, and LC3 protein expression levels. (G) Effect of *R*-Rg3 on cisplatin-induced mitochondrial membrane potential changes. (H) Effect of *R*-Rg3 on cisplatin-induced MPTP opening degree. All values are expressed as mean ± SD (n = 3). $^{**}P < 0.01$, $^{***}P < 0.001$ *vs* normal (N) group; $^{\#}P < 0.05$, $^{\#\#}P < 0.01$, $^{\#\#\#}P < 0.001$ *vs* cisplatin (Cis) group.

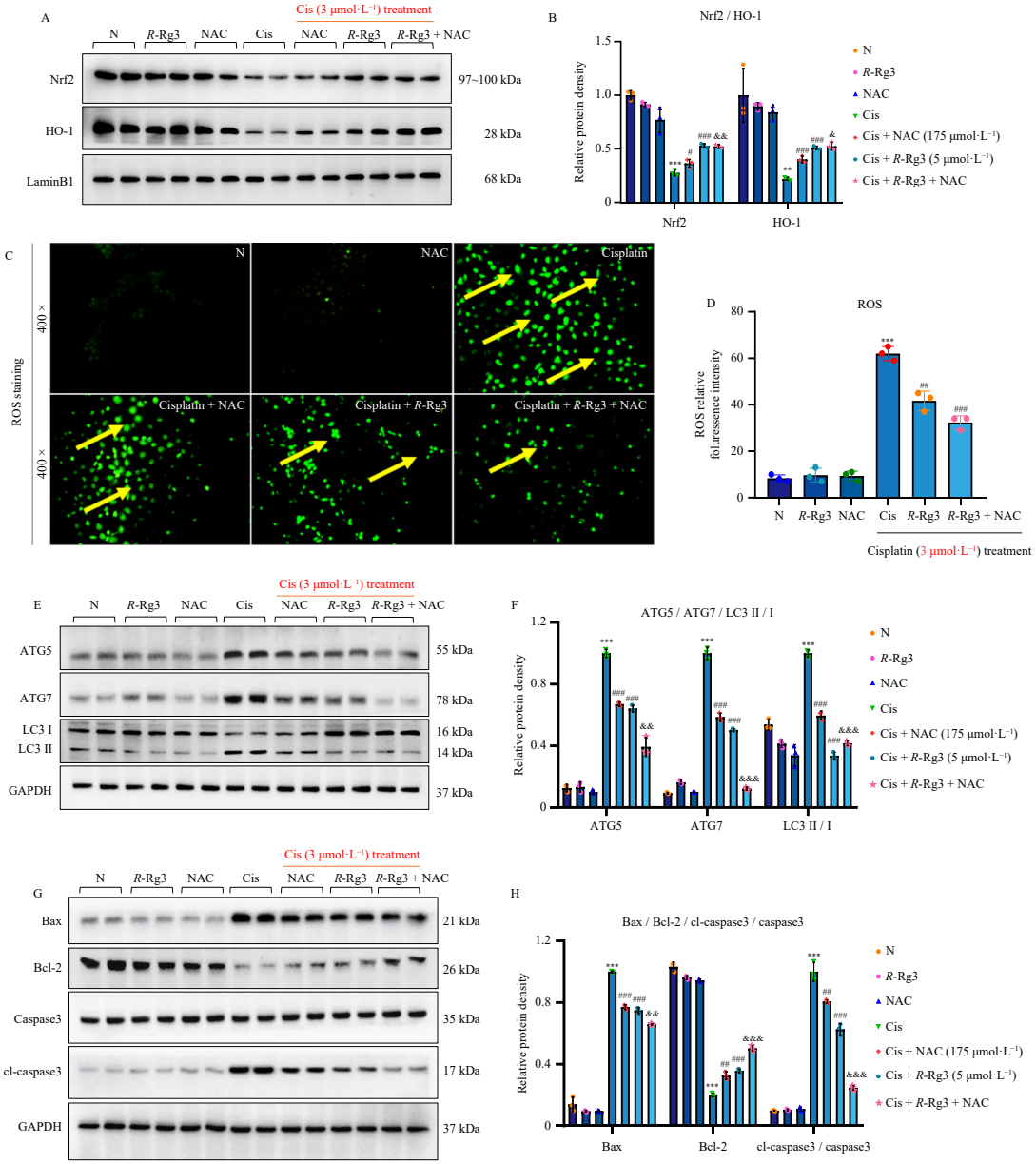

Fig. 5 *R*-Rg3 alleviated mitochondrial dysfunction and autophagic flux by inhibiting ROS accumulation. (A) Effect of *R*-Rg3 plus NAC on protein expression levels of anti-oxidative stress protein. (B) Histogram analysis of Nrf2 and HO-1 protein expression levels. (C) Effect of *R*-Rg3 plus NAC on cisplatin-induced intracellular ROS generation (400 ×). Note: Yellow arrow indicates ROS fluorescence. (D) Histogram analysis of the relative fluorescence intensity of intracellular ROS in each group. (E) Effect of *R*-Rg3 plus NAC on protein expression levels of key proteins in autophagy. (F) Heat map analysis of ATG5, ATG7, and LC3 protein expression levels. (G) Effect of *R*-Rg3 plus NAC on protein expression levels of key proteins in apoptosis. (H) Heat map analysis of Bax, Bcl-2, and cl-caspase 3 protein expression levels. All values are expressed as mean ± SD s Mean ± SD (n = 3 in each group). $^{***}P < 0.001$ *vs* normal (N) group; $^{\#}P < 0.05$, $^{\#\#}P < 0.01$, $^{\#\#\#}P < 0.001$ *vs* cisplatin (Cis) group; $^{\&}P < 0.05$, $^{\&\&}P < 0.01$, $^{\&\&\&}P < 0.001$ *vs* cisplatin + NAC (Cis + NAC) group.

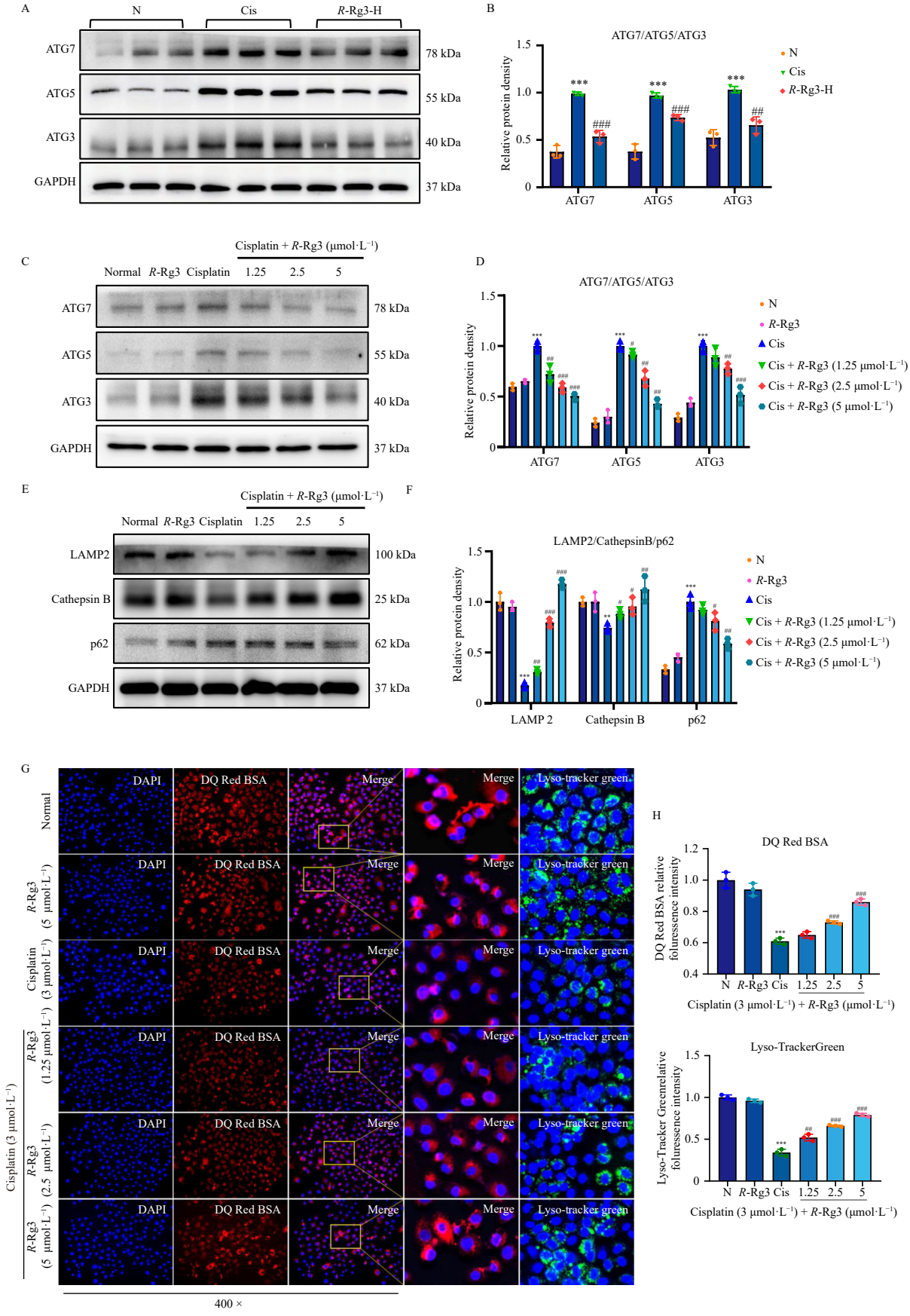

Fig. 6 *R*-Rg3 restrained the excessive autophagy and promoted the restoration of lysosomal function. (A) Effect of *R*-Rg3 on protein expression levels of ATG3, ATG5, ATG7 *in vivo*. (B) Histogram analysis of ATG3, ATG5, ATG7 protein expression levels. (C) Effect of *R*-Rg3 on protein expression levels of ATG3, ATG5, ATG7 *in vitro*. (D) Histogram analysis of ATG3, ATG5, ATG7 protein expression levels. (E) Effect of *R*-Rg3 on protein expression levels of LAMP2, Cathepsin B, p62 *in vitro*. (F) Histogram analysis of LAMP2, Cathepsin B, p62 protein expression levels. (G) Lysosomal function assessment (DQ™ Red BSA/Lyso-Tracker Green) in IEC-6 cells. (H) Histogram analysis of the relative fluorescence intensity of in each group. All values are expressed as mean ± SD (n = 3 in each group). $^{***}P < 0.001$ *vs* normal (N) group; $^{\#}P < 0.05$, $^{\#\#}P < 0.01$; $^{\#\#\#}P < 0.001$ *vs* cisplatin (Cis) group.

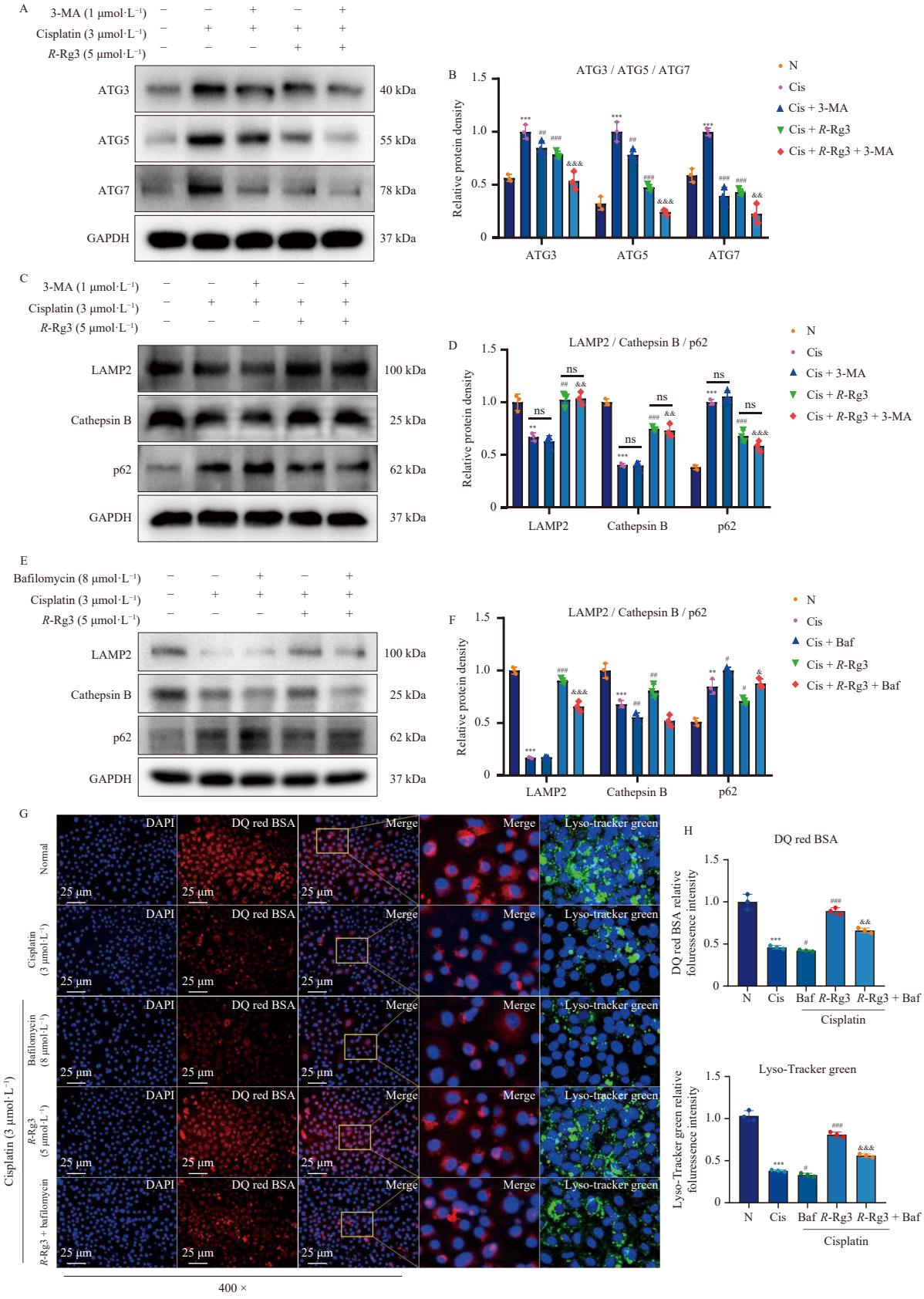

Fig. 7 *R*-Rg3 impeded the cisplatin-induced autophagic flux blockade. (A) Effect of *R*-Rg3 on protein expression levels of ATG3, ATG5, ATG7 in IEC-6 cells by 3-MA. (B) Histogram analysis of ATG3, ATG5, ATG7 protein expression levels. (C) Effect of *R*-Rg3 on protein expression levels of LAMP2, Cathepsin B, p62 in IEC-6 cells by 3-MA. (D) Histogram analysis of LAMP2, Cathepsin B, p62 protein expression levels. (E) Effect of *R*-Rg3 on protein expression levels of LAMP2, Cathepsin B, p62 in IEC-6 cells by Bafilomycin A1. (F) Histogram analysis of LAMP2, Cathepsin B, p62 protein expression levels. (G) Lysosomal function assessment (DQ™ Red BSA/Lyso-Tracker Green) in IEC-6 cells. (H) Histogram analysis of the relative fluorescence intensity of in each group. All values are expressed as mean ± SD (n = 3 in each group). $^{***}P < 0.001$ *vs* normal (N) group; $^{\#}P < 0.05$, $^{\#\#}P < 0.01$, $^{\#\#\#}P < 0.001$ *vs* cisplatin (Cis) group; $^{\&}P < 0.05$, $^{\&\&}P < 0.01$, $^{\&\&\&}P < 0.001$ *vs* cisplatin + 3-MA/Bafilomycin (Cis + 3-MA/Bafilomycin) group.

continuous increase of autophagy [44]. This aberrant activation of autophagy can potentially cause damage and dysfunction to organelles, as critical organelles may be erroneously engulfed within autophagosomes for degradation. Secondly, excessive autophagy may also lead to energy depletion of cells, may eventually trigger cell death, one form of which is through the apoptotic pathway. The effective fusion of lysosomes with autophagosomes is a prerequisite for the clearance of waste from mitochondria [45]. Simultaneously, lysosomal dysfunction can hinder the fusion of autophagosomes with lysosomes, leading to the blockade of autophagic flux. This impediment prevents the effective degradation of autophagosomes, exacerbating the buildup of intracellular waste [46]. In this paper, by introducing autophagy initiation inhibitor 3-MA and proton pump inhibitor Bafilomycin A1, we demonstrated that *R*-Rg3 safeguarded against cisplatin-induced intestinal injury by fostering the restoration of lysosomal function and further alleviating the autophagic flux blockade.

5. Conclusions

In summary, this study not only identified an unrecognized protective role of ginsenoside *R*-Rg3 in cisplatin-induced intestinal injury, but also suggested that pharmacological modulation of *R*-Rg3 on mitochondria-lysosomes may effectively alleviate cisplatin-induced oxidative stress-mediated autophagic flux blockade (Fig. 8).

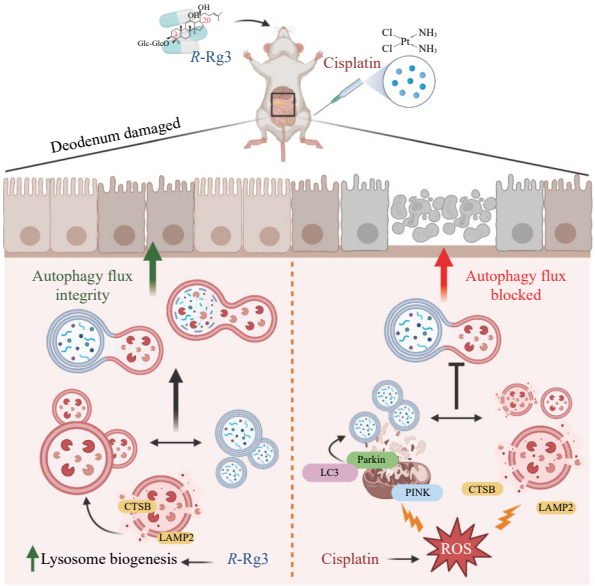

Fig. 8 The molecular mechanism of *R*-Rg3 antagonizing cisplatin-induced intestinal toxicity. Image created with BioRender.com, with permission.

Funding

This work was supported by the National NaturalScience Foundation of China (No. 82474070), the National Key Research and Development Program (No. 2023YFD1601600) and the Science and Technology Research Project of Jilin Provincial Department of Education (No. JJKH20210375KJ).

Declaration of competing interest

The authors declare that there are no conflicts of interest.

References

1 Dasari S, Tchounwou PB. Cisplatin in cancer therapy: molecularmechanisms of action. *Eur J Pharmacol*. 2014;740:364-378. https://doi.org/10.1016/j.ejphar.2014.07.025.
2 Qi LY, Luo Q, Zhang YY, et al. Advances in toxicological research of the anticancer drug cisplatin. *Chem Res Toxicol*. 2019;32(8):1469-1486. https://doi.org/10.1021/acs.chemrestox.9b00204.
3 Soodvilai S, Tipparos W, Rangsimawong W, et al. Effects of silymarin-loaded amphiphilic chitosan polymeric micelles on the renal toxicity and anticanceractivity of cisplatin. *Pharm Dev Technol*. 2019;24(8):927-934. https://doi.org/10.1080/10837450.2018.1556690.
4 Ghosh S. Cisplatin: the first metal based anticancer drug. *Bioorganic Chem*. 2019;88:102925. https://doi.org/10.1016/j.bioorg.2019.102925.
5 Shahid F, Farooqui Z, Khan F. Cisplatin-induced gastrointestinal toxicity: an update on possible mechanisms and on available gastroprotectivestrategies. *Eur J Pharmacol*. 2018;827:49-57. https://doi.org/10.1016/j.ejphar.2018.03.009.
6 Joyce K, Saxena S, Williams A, et al. Antimicrobial spectrum of the antitumor agent, cisplatin. *J Antibiot*. 2010;63(8):530-532. https://doi.org/10.1038/ja.2010.64.
7 Shim HS, Bae C, Wang J, et al. Peripheral and central oxidative stress in chemotherapy-induced neuropathic pain. *Mol Pain*. 2019;15:1744806919840098. https://doi.org/10.1177/1744806919840098.
8 Wang Z, Dong Y, Bai YY, et al. Platycodin D improves early atherosclerosis in type 2 diabetes mellitus by regulating endothelial inflammation and apoptosis. *Am J Chin Med*. 2025:1-26. https://doi.org/10.1142/S0192415X25500703.
9 Suzuki M, Bandoski C, Bartlett JD. Fluoride induces oxidative damage and SIRT1/autophagy through ROS-mediated JNK signaling. *Free Radic BiolMed*. 2015;89:369-378. https://doi.org/10.1016/j.freeradbiomed.2015.08.015.
10 Zhang JJ, Wang JQ, Xu XY, et al. Red ginseng protects against cisplatin-induced intestinal toxicity by inhibiting apoptosis and autophagy *via* the PI3K/AKT and MAPK signaling pathways. *Food Funct*. 2020;11(5):4236-4248. https://doi.org/10.1039/d0fo00469c.
11 Cheng XY, Liang JH, Wu D, et al. Blunting ROS/TRPML1 pathway protects AFB1-induced porcine intestinal epithelial cells apoptosis by restoring impaired autophagic flux. *Ecotox Environ Safe*. 2023;257:114942. https://doi.org/10.1016/j.ecoenv.2023.114942.
12 Mireault M, Xiao Y, Barbeau B, et al. Cadmium affects autophagy in the human intestinal cells Caco-2 through ROS-mediated ERK activation. *Cell Biol Toxicol*. 2023;39(3):945-966. https://doi.org/10.1007/s10565-021-09655-4.
13 Scherz Shouval R, Elazar Z. Regulation of autophagy by ROS: physiologyand pathology. *Trends Biochem Sci*. 2011;36(1):30-38. https://doi.org/10.1016/j.tibs.2010.07.007.
14 Ballabio A, Bonifacino JS. Lysosomes as dynamic regulators of cell and organismal homeostasis. *Nat Rev Mol Cell Biol*. 2020;21(2):101-118. https://doi.org/10.1038/s41580-019-0185-4.
15 Rashid S, Nafees S, Siddiqi A, et al. Partial protection by 18*β*-glycrrhetinic acid against cisplatin induced oxidative intestinal damage in wistar rats: possiblerole of NF-*κ*B and caspases. *Pharmacol Rep*. 2017;69(5):1007-1013. https://doi.org/10.1016/j.pharep.2017.02.013.
16 Shi ZY, Zeng JZ, Wong AS. Chemical structures and pharmacological profiles of *Ginseng* saponins. *Molecules*. 2019;24(13):2443. https://doi.org/10.3390/molecules24132443.
17 Li K, Wang YJ, Chen C, et al. Targeting pyroptosis: a novel strategy of ginseng for the treatment of diabetes and its chronic complications. *Phytomedicine*. 2025;138:156430. https://doi.org/10.1016/j.phymed.2025.156430.
18 Shin JH, Park YJ, Kim W, et al. Change of ginsenoside profiles in processed ginseng by drying, steaming, and puffing. *J Microbiol Biotechnol*. 2019;29(2):222-229. https://doi.org/10.4014/jmb.1809.09056.
19 Peng M, Li XN, Zhang T, et al. Stereoselective pharmacokinetic and metabolism studies of 20(*S*)- and 20(*R*)-ginsenoside Rg_3epimers in rat plasma by liquid chromatography-electrospray ionizationmass spectrometry. *J Pharm Biomed Anal*. 2016;121:215-224. https://doi.org/10.1016/j.jpba.2016.01.020.
20 Li W, Wang JQ, Zhou YD, et al. Rare ginsenoside 20(*R*)-Rg3 inhibits D-galactose-induced liver and kidney injury by regulating oxidative stress-induced apoptosis. *Am J Chin Med*. 2020;48(5):1141-1157. https://doi.org/10.1142/s0192415x20500561.
21 Sha JY, Zhou YD, Yang JY, et al. Maltol (3-hydroxy-2-methyl-4-pyrone) slows D-galactose-induced brain aging process by damping the Nrf2/HO-1-mediated oxidative stress in mice. *J Agric Food Chem*. 2019;67(37):10342-10351. https://doi.org/10.1021/acs.jafc.9b04614.
22 Zhang JJ, Zhou YD, Liu YB, et al. Protective effect of 20(*R*)-ginsenoside Rg3 against cisplatin-induced renal toxicity *via* PI3K/AKT and NF-*κ*B signaling pathways based on the premise of ensuring anticancer effect. *Am J Chin Med*. 2021;49(07):1739-1756. https://doi.org/10.1142/s0192415x21500828.
23 Hu JN, Yang JY, Jiang S, et al. *Panax quinquefolium* saponins protect against cisplatin evoked intestinal injury *via* ROS-mediated multiple mechanisms. *Phytomedicine*. 2021;82:153446. https://doi.org/10.1016/j.phymed.2020.153446.
24 Xing JJ, Hou JG, Ma ZN, et al. Ginsenoside Rb3 provides protective effects against cisplatin-induced nephrotoxicity *via* regulation of AMPK-/mTOR-mediated autophagy and inhibition of apoptosis *in vitro* and *in vivo*. *Cell Prolif*. 2019;52(4):e12627. https://doi.org/10.1111/cpr.12627.
25 Zhang JJ, Chen KC, Zhou Y, et al. Evaluating the effects of mitochondrial autophagy flux on ginsenoside Rg2 for delaying D-galactose induced brain aging in mice. *Phytomedicine*. 2022;104:154341. https://doi.org/10.1016/j.phymed.2022.154341.
26 Zhang YB, Sun H, Pei RJ, et al. The SARS-CoV-2 protein ORF3a inhibits fusion of autophagosomes with lysosomes. *Cell Discov*. 2021;7(1):31. https://doi.org/10.1038/s41421-021-00268-z.
27 Saad AA, Youssef MI, El-Shennawy LK. Cisplatin induced damage in kidney genomic DNA and nephrotoxicity in male rats: the protective effect of grape seed proanthocyanidin extract. *Food Chem Toxicol*. 2009;47(7):1499-1506. https://doi.org/10.1016/j.fct.2009.03.043.
28 Wu CH, Ko JL, Liao JM, et al. D-methionine alleviates cisplatin-induced

mucositis by restoring the gut microbiota structure and improving intestinal inflammation. *Ther Adv Med Oncol*. 2019;11:1758835918821021. https://doi.org/10.1177/1758835918821021.
29 Del Re M, Latiano T, Fidilio L, et al. Unusual gastrointestinal and cutaneous toxicities by bleomycin, etoposide, and cisplatin: a case report with pharmacogenetic analysis to personalize treatment. *Epma J*. 2017;8(1):69-73. https://doi.org/10.1007/s13167-017-0080-z.
30 Chang BJ, Nishikawa M, Sato E, et al. L-Carnitine inhibits cisplatin-induced injury of the kidney and small intestine. *Arch Biochem Biophys*. 2002;405(1):55-64. https://doi.org/10.1016/s0003-9861(02)00342-9.
31 Li BW, Wang WZ, Li Z, et al. Micro RNA-148a-3p enhances cisplatin cytotoxicity in gastric cancer through mitochondrial fission induction and cyto-protective autophagy suppression. *Cancer Lett*. 2017;410:212-227. https://doi.org/10.1016/j.canlet.2017.09.035.
32 Guerrero-Beltran CE, Calderon-Oliver M, Martinez-Abundis E, et al. Protective effect of sulforaphane against cisplatin-induced mitochondrial alterations and impairment in the activity of NAD(P)H: quinone oxidoreductase 1 and γ glutamyl cysteine ligase: studies in mitochondria isolated from rat kidney and in LLC-PK1 cells. *Toxicol Lett*. 2010;199(1):80-92. https://doi.org/10.1016/j.toxlet.2010.08.009.
33 Xiao L, Cui T, Liu S, et al. Vitamin A supplementation improves the intestinal mucosal barrier and facilitates the expression of tight junction proteins inrats with diarrhea. *Nutrition*. 2019;57:97-108. https://doi.org/10.1016/j.nut.2018.06.007.
34 Obermeier B, Daneman R, Ransohoff RM. Development, maintenance and disruption of the blood-brain barrier. *Nat Med*. 2013;19(12):1584-1596. https://doi.org/10.1038/nm.3407.
35 Al-Sadi R, Khatib K, Guo S, et al. Occludin regulates macromolecule flux across the intestinal epithe lial tight junction barrier. *Am J Physiol Gastroint Liver Physiol*. 2011;300(6):G1054-G1064. https://doi.org/10.1152/ajpgi.00055.2011.
36 Hazman O, Bozkurt MF, Fidan AF, et al. The effect of boric acid and borax on oxidative stress, inflammation, ER stress and apoptosis in cisplatin toxication and nephrotoxicity developing as a result of toxication. *Inflammation*. 2018;41(3):1032-1048. https://doi.org/10.1007/s10753-018-0756-0.
37 Ma ZN, Li YZ, Li W, et al. Nephroprotective effects of saponins from leaves of *Panax quinquefolius* against cisplatin-induced acute kidney injury. *Int J Mol Sci*. 2017;18(7):1407. https://doi.org/10.3390/ijms18071407.
38 Ni YD, Zhu YY, Xu LX, et al. Pharmacological activities and mechanisms of proteins and peptides derived from traditional Chinese medicine. *Sci Tradit Chin Med*. 2024;2(4):260-275. https://doi.org/10.1097/st9.0000000000000054.
39 Deshmukh P, Unni S, Krishnappa G, et al. The Keap1-Nrf2 pathway: promising therapeutic target to counteract ROS-mediated damage in cancersand neurodegenerative diseases. *Biophys Rev*. 2017;9(1):41-56. https://doi.org/10.1007/s12551-016-0244-4.
40 Luo Q, Peng B, Wei XL, et al. Research progress of Chinese herbal medicines and classic prescriptions in the treatment of COPD based on theTCM theoryand medicinal characteristics. *Sci Tradit Chin Med*. 2024;2(2):104-120. https://doi.org/10.1097/st9.0000000000000028.
41 Lu YW, Xie LY, Qi MH, et al. Platycodin D ameliorates cognitive impairment in type 2 diabetes mellitus mice *via* regulating PI3K/Akt/GSK3β signalingpathway. *J Agric Food Chem*. 2024;72(22):12516-12528. https://doi.org/10.1021/acs.jafc.3c08490.
42 Yoshii SR, Mizushima N. Autophagy machinery in the context of mammalian mitophagy. *Biochim Biophys Acta*. 2015;1853(10):2797-2801. https://doi.org/10.1016/j.bbamcr.2015.01.013.
43 Mcwilliams TG, Muqit MMK. PINK1 and Parkin: emerging themes in mitochondrial homeostasis. *Curr Opin Cell Biol*. 2017;45:83-91. https://doi.org/10.1016/j.ceb.2017.03.013.
44 Galluzzi L, Baehrecke EH, Ballabio A, et al. Molecular definitions of autophagy and related processes. *Embo J*. 2017;36(13):1811-1836. https://doi.org/10.15252/embj.201796697.
45 Settembre C, Fraldi A, Medina DL, et al. Signals from the lysosome: a control centre for cellular clearance and energy metabolism. *Nat Rev Mol Cell Biol*. 2013;14(5):283-296. https://doi.org/10.1038/nrm3565.
46 Yu L, Chen Y, Tooze SA. Autophagy pathway: cellular and molecular mechanisms. *Autophagy*. 2018;14(2):207-215. https://doi.org/10.1080/15548627.2017.1378838.